Iontophoresis From a Micropipet into a Porous Medium Depends on the ζ-Potential of the Medium

ARTICLE *in* ANALYTICAL CHEMISTRY · MARCH 2012

Impact Factor: 5.64 · DOI: 10.1021/ac202434c · Source: PubMed

5 AUTHORS, INCLUDING:

Amir Faraji
University of Pittsburgh
16 PUBLICATIONS **354** CITATIONS
SEE PROFILE

Timothy G Strein
Bucknell University
33 PUBLICATIONS **624** CITATIONS
SEE PROFILE

Stephen Gregory Weber
University of Pittsburgh
233 PUBLICATIONS **3,560** CITATIONS
SEE PROFILE

Published in final edited form as:
Anal Chem. 2012 March 6; 84(5): 2179–2187. doi:10.1021/ac202434c.

Iontophoresis From a Micropipette into a Porous Medium Depends on the ζ-Potential of the Medium

Yifat Guy[†], **Amir H. Faraji**[†], **Colleen A. Gavigan**[‡], **Timothy G. Strein**[‡], and **Stephen G. Weber**[†,*,†]

[†]Department of Chemistry, University of Pittsburgh, Pittsburgh, PA 15260.

[‡]Department of Chemistry, Bucknell University, Lewisburg, PA 17837.

Abstract

Iontophoresis uses electricity to deliver solutes into living tissue. Often, iontophoretic ejections from micropipettes into brain tissue are confined to millisecond pulses for highly localized delivery, but longer pulses are common. As hippocampal tissue has a ζ-potential of approximately –22 mV, we hypothesized that, in the presence of the electric field resulting from the iontophoretic current, electroosmotic flow in the tissue would carry solutes considerably farther than diffusion alone. A steady state solution to this mass transport problem predicts a spherically symmetrical solute concentration profile with the characteristic distance of the profile depending on the ζ-potential of the medium, the current density at the tip, the tip size and the solute electrophoretic mobility and diffusion coefficient. Of course, the ζ-potential of the tissue is defined by immobilized components of the extracellular matrix as well as cell-surface functional groups. As such, it cannot be changed at will. Therefore, the effect of the ζ-potential of the porous medium on ejections is examined using poly(acrylamide-*co*-acrylic acid) hydrogels with various magnitudes of ζ-potential, including that similar to hippocampal brain tissue. We demonstrated that nearly neutral fluorescent dextran (3 and 70 kD) solute penetration distance in the hydrogels and OHSCs depends on the magnitude of the applied current, solute properties, and, in the case of the hydrogels, the ζ-potential of the matrix. Steady state solute ejection profiles can be predicted semi-quantitatively.

Keywords

Electroosmosis; Peclet number; Mass transport; Hippocampus; Microiontophoresis

Iontophoresis is a method of introducing solutes into tissue using an electrical current. This technique has seen wide clinical application in the delivery of bioactive compounds, mostly through skin.[1] In early work, the technique was used to deliver ions according to their charge and the sign of the current. While electrophoresis certainly occurs, several authors have pointed out the importance of electroosmotic flow in the skin to the overall rate of iontophoretic delivery to the tissue below the skin.[2-5] Electroosmotic flow enhances the delivery of cationic and neutral solutes, and decreases the delivery of anions. Reverse iontophoresis in skin, for example to obtain samples for determination of glucose, is also assisted by electroosmosis.[6] Transocular iontophoresis is similarly thought to involve electroosmosis.[7] In the foregoing applications and the related experimental research work,

*Corresponding author: Tel +1 412-624-8520, Fax +1 412-624-8611, sweber@pitt.edu.

Supporting Information Available

Discussion of time to steady state; Summary table of data; Experimental details on fluorophores; Circuit diagrams for triggering current source.

the geometry of the system is similar to a planar membrane (skin, corneal surface, etc.) separating a pair of chambers, each containing an electrode. The area through which current flows is similar to the area of tissue into which drug is delivered, so macroscopically the current density (electric field divided by conductivity) is approximately constant.

Iontophoresis can also be carried out from a source that is small compared to the size of the affected region, e.g., iontophoresis from a micropipette.[8] This type of iontophoresis, which is sometimes referred to as microiontophoresis, has helped to reveal the brain's physiological and physicochemical properties and transport mechanisms.[9] Attempts to quantify iontophoretic ejections from pipettes into tissue have had limited success.[10-12] Researchers have used ion-selective microelectrodes,[13-16] carbon fiber microelectrodes, [17-19] and fluorescence microscopy[20] to measure solute ejection outside of the ejection pipette. Yet an understanding of what parameters control the distribution of solute in iontophoresis in a porous medium like tissue remains elusive. Trubatch and Van Harreveld proposed that electrokinetic processes within the tissue, e.g., electroosmosis, may account for some of the lack of agreement between predicted and experimental ejection profiles.[21] This notion was quickly refuted by Norman and others who stated that pulsed iontophoretic currents are too low (≤100 nA) and ejections are too short to create appreciable electrokinetic contributions within the tissue.[22-24] An important part of the argument against the presence of a significant impact of electroosmosis relates to the geometry mentioned above. Unlike the macroscopically “planar” geometry described above for skin iontophoresis, the current density and electric field decay rapidly from a point, circular, or spherical source of current when the counter electrode is distant from the source. Also, in iontophoresis from a small source like a pipette especially for short current pulses, the delivered volume is small, so diffusion may be the predominant route of mass transport as it often is at short times over small distances. Thus, there is reason to be skeptical about the role of electroosmosis in iontophoresis from a micropipette. Until recently, the standard view was that iontophoresis into the brain from a micropipette can only convey charged solutes into tissue via solute migration in the iontophoretic pipette and diffusion thereafter in the tissue.[22-26]

Recently, Herr *et al.* showed that electroosmotic flow (EOF) *in the pipette* makes a significant contribution to iontophoretic ejections into buffer solution.[27] As a result of the EOF in the pipette, a neutral solute could be ejected.[19,27] We have recently reported that rat organotypic hippocampal cultures have a ζ-potential of approximately -22 mV.[28,29] Xu *et al.* were able to show sustained EOF in brain tissue to acquire samples of extracellular fluid.[30] We propose that, under many conditions used experimentally, solute transport from a pipette into brain tissue can be influenced by the ζ-potential of brain tissue and the resulting EOF in the tissue.

Theory

The Peclet number, Pe, is defined in eq 1 in which ‘a’ is a characteristic distance, v is a velocity, and D is a diffusion coefficient.

$$\mathrm{Pe}=\frac{v\mathrm{a}}{D} \tag{1}$$

Solute velocity, v, contains three components: an electrophoretic velocity, v_{ep}, an electroosmotic velocity, v_{eo}, and a pressure-induced velocity, v_p. We assume that v_p is small compared to v_{ep} and v_{eo}, and therefore is not accounted for in this derivation. Each of the remaining two velocities is governed by the magnitude of the electric field. Eq 2 relates the electric field, E, to the current applied to the system, i:

$$E=\frac{j}{g_E}=\frac{i}{\mathrm{A}\quad g_E} \tag{2}$$

where j is the current density, g_E is the conductivity of the fluid, and A is the cross-sectional area (see Figure 1).

Eqs 3 and 4 define electrophoretic and electroosmotic velocities as products of electric field and the corresponding mobility, μ.

$$v_{\mathrm{ep}}=\mu_{\mathrm{ep}}E \tag{3}$$

$$v_{\mathrm{eo}}=\mu_{\mathrm{eo}}E=\left(-\varepsilon\zeta\Big/\eta\right)E \tag{4}$$

$$v=v_{\mathrm{ep}}+v_{\mathrm{eo}}=\left(\mu_{\mathrm{ep}}+\mu_{\mathrm{eo}}\right)E=\mu_{\mathrm{obs}}E \tag{5}$$

Eq 4 shows that the electroosmotic velocity is a function of the ζ-potential of the matrix (ζ), and the permittivity (ε) and viscosity (η) of the fluid. Eq 5 relates the observed mobility, μ_{obs}, to the sum of the electroosmotic and electrophoretic velocities. Incorporating eqs 2 through 4 into eq 1 yields a theoretical calculation of Pe, $\mathrm{Pe_T}$, in eq 6 based on measurable quantities.

$$\mathrm{Pe_T}=\frac{i\cdot \mathrm{a}}{\mathrm{A}\cdot g_E\cdot D}\mu_{\mathrm{obs}}=\frac{i\cdot\mu_{\mathrm{obs}}}{2\pi\cdot \mathrm{a}\cdot g_E\cdot D} \tag{6}$$

The first eq 6 in terms of area, A, is quite general. In the case of iontophoresis, from a micropipette solute emanates from an orifice into a much larger medium. For mathematical simplicity, we will consider the solute to be emanating from a hemisphere (this leads to $\mathrm{A}=2\pi\mathrm{a}^2$, and thus the final eq 6). The radius of the hemisphere, a, appears in $\mathrm{Pe_T}$, and is used as a normalizing factor for distance r: ρ = r/a (Figure 1). The steady state concentration profile of a solute diffusing from a hemispherical source takes on the familiar shape described by eq 7[31]. The concentration, C, is a function of distance, r, and $\mathrm{C_0}$ = C (r = a).

$$\mathrm{C}=\mathrm{C_0}\frac{\mathrm{a}}{\mathrm{r}}=\frac{\mathrm{C_0}}{\rho} \tag{7}$$

When fluid convection and electrophoresis as well as diffusion contribute to the flux, we can solve for the steady state condition in the hemispherical coordinate system as follows. Eq 8 describes solute flux:

$$J=\mathrm{C}v-D\nabla\mathrm{C} \tag{8}$$

where J is the flux of solute, v is the velocity of the solute due to fluid convection and electrophoresis, and the last term on the right side is the diffusional flux resulting from a concentration gradient. We assume that the electric field distribution from the pipette tip is equal to the field distribution from a hemispherical electrode, i.e., $E\,(\mathrm{r})=\frac{\mathrm{a}^2}{\mathrm{r}^2}E_0$ where E_0 is the field at r = a, leading to eq 9.

$$J = \mathrm{C}(\mathrm{r})\,\mu_{\mathrm{obs}}\frac{\mathrm{a}^2}{\mathrm{r}^2}E_0 - D\frac{d\mathrm{C}(\mathrm{r})}{d\mathrm{r}} \tag{9}$$

Note that in the case of no electric field the flux is governed solely by the diffusion of the solute. Steady state is achieved in a spherical coordinate system when $\mathrm{d}(\mathrm{r}^2 J)/\mathrm{dr} = 0$. Thus, eq 10 describes the steady state condition. Eq 11 results from replacing *dC/dr* with *C'*, d^2C/dr^2 with *C"*, and rearranging eq 10.

$$\mu_{\mathrm{obs}}E_0\mathrm{a}^2\frac{d\mathrm{C}}{d\mathrm{r}} - 2\mathrm{r}D\frac{d\mathrm{C}}{d\mathrm{r}} - \mathrm{r}^2 D\frac{d^2\mathrm{C}}{d\mathrm{r}^2} = 0 \tag{10}$$

$$\left(\frac{\mathrm{Pe}_E}{\rho^2} - \frac{2}{\rho}\right)C' = C'' \tag{11}$$

Here Pe_E is based on the electric field at the tip ($\rho = 1$), i.e,

$$\mathrm{Pe}_E = \frac{\mu_{\mathrm{obs}}E_0\mathrm{a}}{D} \tag{12}$$

Eq 11 can be solved by solving the first order differential eq for the function F = *C'*, and then solving the resulting eq for *C'* by integration with boundary conditions:

Boundary Condition 1: $\mathrm{C}(\rho \to \infty) = 0$

Boundary Condition 2: $\mathrm{C}(\rho \to 1) = \mathrm{C}_0$

$$\mathrm{C}(\rho) = \mathrm{C}_0\left(\frac{1 - e^{-\mathrm{Pe}_E/\rho}}{1 - e^{-\mathrm{Pe}_E}}\right) \tag{13a}$$

When the electrokinetic effects are negligible, Pe_E tends to zero. Expanding the exponentials as Taylor series and truncation of quadratic and higher order terms leads to the recovery of eq 7. We note that, while it is easy to assert that boundary condition 2 above exists, it is very hard to know the value of C_0 in practice. This problem is not resolved by using a constant flux boundary condition in which case the solution is

$$\mathrm{C}(\rho) = \frac{J_0\mathrm{a}}{\mathrm{Pe}_E D}\left(1 - e^{-\mathrm{Pe}_E/\rho}\right) \tag{13b}$$

In other words,

$$\mathrm{C}_0 = \frac{J_0\mathrm{a}}{\mathrm{Pe}_E D\left(1 - e^{-\mathrm{Pe}_E}\right)} \tag{13c}$$

We cannot determine the flux at the tip, J_0, either. Thus, the derivation provides the shape of the concentration profile to be expected, but not the magnitude.

We hypothesize that a larger magnitude tissue ζ-potential will be associated with larger ejection distance in a given time period. As a tissue's ζ-potential cannot be altered, we will test this hypothesis using synthetic poly(acrylamide-*co*-acrylic acid) hydrogels as tissue models with varying ζ-potentials[32]. We examine the degree of fluorescent dextran solute penetration as a function of matrix ζ-potential and applied current. By understanding the EOF in both the delivery system and in the tissue itself, we can in principle estimate the ejected solute distribution.

Experimental Section

Chemicals and Solutions

Unless otherwise noted, the following materials were purchased from Sigma (St. Louis, MO) and used as received. Solutions were prepared with Millipore Synthesis A10 system 18 MΩ-cm purified water (Millipore, Billerica, MA). Glucose-free HEPES-buffered salt solution (G-f HBSS) contained in mM: 143.4 NaCl, 5 HEPES, 5.4 KCl, 1.2 $MgSO_4$, 1.2 NaH_2PO_4, and 2.0 $CaCl_2$. G-f HBSS was filtered, stored frozen, warmed to room temperature, and ultrasonicated for ten minutes before use. HBSS contained the same quantities as G-f HBSS with an additional 10 mM D-(+)-glucose and underwent the same preparation and storage process. GBSS was made up of 27.5 mM D-(+)-glucose and filtered 2.7 mM $MgSO_4$ supplemented Gey's Balanced Salt solution. GBSS was stored in the refrigerator and warmed to 37 °C before use.

Culture medium contained the following from Gibco (Invitrogen, Eugene, OR): 50 % Opti-MEM, 25 % heat-inactivated Horse Serum, and 25 % Hank's Balanced Salt Solution, supplemented with 2 % B-27 vitamin and 1 % D-(+)-glucose from Sigma.[33] Medium was filtered, refrigerated for storage, and warmed to 37 °C before use.

Determination of Diffusion Coefficients and Electrophoretic Mobilities in Free Solution

Diffusion coefficients in free solution were determined as described in Beisler *et al*.[3] G-f HBSS mobile phase was pumped through a thermostated capillary using a Pico Plus syringe pump (Harvard Apparatus, Holliston, MA). The sample solutions were injected using an HP 1050 autosampler (Hewlett-Packard, Palo Alto, CA) into a 1 μL loop in a VICI 6-port Cheminert Injector (Houston, TX). The detector from an ISCO 3850 Capillary Electropherograph (Teledyne ISCO, Lincoln, NE) was used for UV detection (215 nm) of the fluorophores. Signals were collected by Peaksimple 3.29 (SRI Inc., Torrance, CA) for analysis. Data were imported into Origin 7.5 (Origin Lab Cooperation, Northampton, MA) for differentiation, followed by the determination of the first and second central moments using PeakFit version 4 (Systac Software Inc., San Jose, CA). Diffusion coefficients were calculated from the slopes of second moment versus first moment linear plots. In addition, errors for the diffusion coefficients were calculated based on the error of the slope, assuming negligible error in the flow rate, capillary length and capillary diameter.

The electrophoretic mobilities of the fluorophores in G-f HBSS were determined via CZE with diode array UV absorbance detection using 50 μm inner diameter (ID) capillaries and an Agilent CE system (Agilent Technologies, Palo Alto, Ca). Hydrodynamic injection (25 mbar, 4 second) was employed, and all experiments were performed at 25°C. For **TR3** (595 nm) and $Ru(bpy)_3^{2+}$ (452 nm) an unmodified fused silica capillary (Polymicro Technologies, Phoenix, AZ) was employed. The capillary was preconditioned with 1 M NaOH for 15 minutes, 18 MΩ-cm water for 15 minutes and G-f HBSS for 15 minutes, and was flushed with running buffer for 2 minutes in between injections. Rhodamine B (544 nm) was used as a neutral flow marker. The capillary was 33.0 cm in total length, 8.5 cm to the detector, and the separation voltage was 6.0 kV (182 V/cm). Fluorophores were dissolved in G-f HBSS and had concentrations ranging from 0.3 to 1.7 mM.

Organotypic Hippocampal Slice Cultures (OHSCs)

The organotypic hippocampal slice culture (OHSC) method, developed by Stoppini *et al.* was used with slight variations. [34] The following procedures were approved by the University of Pittsburgh IACUC. Bilateral dissections of the hippocampi were done on 9-day postnatal Sprague-Dawley albino rats. The hippocampi were chopped along the transverse axis to 350 μm thick slices using a McIlwain tissue chopper (The Mickle Latoratory Engineering, Surrey, England). The slices were placed on 0.4 μm PTFE insert membranes (Millipore, Bedford, MA) and incubated over 1.2 mL of medium at 36.5 °C in 5 % CO_2/ 95 % air for 6 to 8 days. Culture medium was exchanged every 2 to 3 days. Prior to experiments, culture medium was replaced with 37 °C GBSS and incubated for thirty minutes. A second GBSS exchange followed for another incubation period of 30 minutes. A last exchange to 37 °C HBSS and incubation for 30 minutes was done prior to experimental use.

Electrokinetic Ejections into Hydrogels

Borosilicate pipettes with filaments (1 mm × 0.58 mm, 4 inches long) (A-M Systems, Inc., Carlsborg, WA) were pulled using the Sutter P-2000 capillary puller to tips of approximately 2 μm inner radii. Tip size and shape were measured using an Olympus BX41 optical microscope. Figure 2 diagrams the 0.64 cm thick PVC cell that held the hydrogel pieces. It has a 1 × 1 × 0.64 cm^3 space in its center and a 1 mm wide × 1 mm high × 2.2 cm long channel milled at its base on either side of the center space. The cell was secured on an Olympus IX81 inverted fluorescence microscope stage and imaged with a high resolution charged-coupled device camera (ORCA-ER).

Hydrogel sections were cut to size and placed in the cell. The pulled borosilicate pipette was placed through one of the channels into the hydrogel. A silver wire ground electrode (0.3 mm diameter) was inserted a few millimeters into the hydrogel through the other channel. The distance between the pipette tip and the ground electrode was always more than 3.5 mm. A second Ag wire, which is called the working electrode, was inserted into the back end of the pipette. The current source was either a Digital Midgard™ Precision Current Source iontophoretic pump (Stoelting Co., Wood Dale, IL) or a Princeton Applied Research 173 galvanostat (PAR) (Princeton, NJ). The current source was attached to the electrodes through a software-controlled switch (see SI, Figure S3). Image sequences were acquired using MetaMorph 7.6.2.0 software (MDS Analytical Technologies, Sunnyvale, CA) using one of the following Olympus objective lenses: UPlan Fl 4×, UPlan S Apo 10×, or a long working distance LUCPlan Fl N 40×. The PAR was used for Texas Red dextran conjugate 70 kDa (**TR70**) ejections with currents of less than 1 μA, although the Midgard™ pump was used for some ejections at 0.5 μA. The PAR setup included a 0.3 mm diameter platinum (Pt) electrode as the working electrode. Currents were applied for 270 to 840 seconds, depending on estimated times to steady state.

Image sequences were analyzed by drawing a line scan from the center of the pipette tip to the end of the field of view on the same axis as the pipette. Intensity data were recorded along the line scan before the initiation of current (background intensity), and at 30 second intervals after the current was applied. Background intensity was subtracted from line scan intensities. Since concentration is related to intensity measured, we can replace concentration, C, in eq 12 with intensity, I. Reported intensity values are between 0 and 4095. Values of I_0, I_1, and Pe_E were determined by nonlinear fitting of eq 14 to data with Mathcad 14 (PTC, Needham, MA). I_1 is included to correct for baseline intensity.

$$I(\rho) = I_0 \left(\frac{1 - e^{-Pe_E/\rho}}{1 - e^{-Pe_E}} \right) + I_1 \quad (14)$$

Electrokinetic Ejections into OHSCs

Experiments in the OHSC were set up as shown in Figure 3 with the Digital Midgard™ iontophoresis pump. An insert membrane with an OHSC was placed in a dish with HBSS. A silver ground electrode was remotely secured, such that it made contact with the HBSS bath. A pulled borosilicate pipette filled with fluorophore solution and containing a silver electrode was positioned at a 20° angle using a manipulator arm on a Narishige NMN-21 micromanipulator (Tokyo, Japan). The tip was inserted into the CA1 region of the OHSC. The electrode circuitry is the same as the hydrogel experiment. A current of 0.5 μA was applied using the iontophoresis pump for 270 seconds for OHSC experiments.

OHSCs analyzed for cell death following ejection were subjected to identical conditions, with the exception that the ejection solution only contained HBSS, without fluorophore, to avoid interference with propidium iodide (PI) fluorescence. Following the experiment, OHSCs were incubated for 24 hours over culture medium supplemented with PI (final concentration of 7 μM). Positive cell death controls were subjected to a drop of methanol placed on top of the OHSCs prior to the 24 hour incubation with PI.[35] Negative controls were subjected to the same procedure as experimental OHSCs, without placement of the pipette and application of current. Following incubation, the medium was exchanged with the same GBSS-GBSS-HBSS procedure described earlier and imaged on the IX81 inverted fluorescence microscope with the 4× UPlan Fl objective lens. PI was imaged using a 560/25 excitation filter, a 625/26 emission filter, both obtained from Olympus, and the Semrock triple-band dichroic mirror described earlier. A circular region of interest (50 μm^2) was used to measure the average intensity within the area of injection. Cell death was analyzed as described by Hamsher et al.[35] Briefly, PI intensities of OHSCs used in ejection experiments were scaled to positive (100% cell death) and negative (0% cell death).

Results and Discussion

Properties of the fluorophores, hydrogels, and iontophoresis pipettes

Table 1 summarizes the free solution diffusion coefficients and mobilities of the fluorophores. These measurements were all made by the procedures described in the experimental section, although some were reported previously and are so indicated in the table. As described in detail above, the mobilities were determined by capillary electrophoresis, and the diffusion coefficients were determined by a Taylor dispersion method. We note that the mobilities of the dextran conjugates are fairly small and positive.

To assess the relative importance of electrophoresis vs. electroosmosis for the solutes used here, we have tabulated the ratio of the electroosmotic mobility of the hydrogels to the electrophoretic mobility of the respective solute in Table S1. All of these ratios are significantly greater than unity except for two – **TR70** and **TR3** in the near-zero ζ-potential hydrogel. Thus, with these exceptions, electric-field- dependent dextran transport is dominated by electroosmosis in the hydrogels. Nonetheless, in calculating Pe_T (eq 6), we include the electrophoretic mobility.

While our focus here is on the influence of the ζ-potential of the medium, we must consider the effect of the pipette's ζ-potential. Herr *et al.* [27] were able to quantify iontophoretic solute

ejections into free solution relative to a neutral marker. They included a discussion of the effects of ionic strength and pH on the pipette ζ-potential. Using that information with our electrolyte conditions (G-f HBSS: pH 7.4, ionic strength ≈ 0.15 M), we estimate the pipette ζ-potential to be approximately -10 mV. This value agrees with the literature on other objects made of borosilicate glass[36-38]. This also agrees with our experimental observation that the pipette ζ-potential must be more positive than -11 mV. If the ζ- potential of the pipette had been more negative, then we would have observed ejection of fluorescein dextran conjugate 70 kDa ($\mu_{ep} = -8.8 \times 10^{-9}$ m^2/Vs) from the pipette, but we do not (data not shown).

The experimental conditions that are fixed for a given measurement in a hydrogel are the ζ-potential of the hydrogel, the current applied, the fluorescent solute used, and the tip diameter. For a given experiment in a hydrogel, a large number of pipettes are pulled, all of which have the same tip dimensions. There is some day-to-day variability, however. Furthermore, the tips in each set tended to be elliptical. The long dimension for twelve sets of pipettes (rows 1-12 in Table S1) ranged from 4.0 – 4.2 μm, heavily skewed to the smaller end (mean: 4.0_3 μm). The short dimension for the same sets ranged from 3.9 to 2.2 μm, skewed to the larger dimension (mean: 3.6_2 μm). The radius, a, used to calculate the value of Pe_T for a particular experiment is one-half of the geometrical mean of the long and short diameters befitting the elliptical tip shape. The thirty-one experiments on tissue cultures took place on several days over an extended period, so unlike the experiments with hydrogels, pipettes with slightly different sizes were used. The value of a for these pipettes ranged from 1.9 to 2.2 μm with a mean of 2.03 μm and an SEM of 0.02 μm.

The hydrogels that we used had a range of ζ-potentials from approximately 0 to -25 mV (actual values given with data).[32] Two juxtaposed media with different ζ-potentials create pressure in an electric field.[39] When the hydrogel's ζ-potential magnitude is less than that of the capillary, there is the possibility of transport by pressure-induced flow arising from the larger ζ-potential in the pipette. When the hydraulic permeability is high in the medium with the larger ζ-potential magnitude (pipette), and the hydraulic permeability is low in the medium with the smaller ζ-potential magnitude (hydrogel), pressure-induced fluid flow in the hydrogel is likely to be small.[40] Eq 13 does not take this into account. As discussed below, it is likely that some pressure-flow exists in the hydrogels.

Experimental intensity-distance profiles in hydrogels

Individual experimental intensity-distance profiles were converted to intensity-ρ profiles by dividing experimental distances by the tip radius for the particular experiment. Nonlinear fitting of eq 14 to intensity vs. distance data yielded values of Pe_E. Of 120 individual hydrogel intensity-distance curves, nine were not used because of the low correlation coefficients (< 0.98) from the fit of eq 14 to the experimental intensity profiles. Because of the expectation of increased variability in tissue experiments, all thirty-one experiments in OHSCs were used (correlation coefficient > 0.89). We have chosen to represent the average concentration profile for a given set of conditions by using average values of characteristic distances corresponding to $I(\rho)/I_0 = 1$, 0.75, 0.50, and 0.25. Figure 4 shows the average characteristic distances and intensity profiles from steady state (or near steady state; see SI) iontophoretic ejections of **TR70** and **TR3** in hydrogels. The penetration distance of the ejection (Figure 4) clearly depends on the ζ-potential and thus the EOF in the porous medium. The influence of EOF in each hydrogel is most clearly seen in the data from the nearly neutral solute, **TR70** (Figure 4a). Higher magnitude ζ-potentials result in greater EOF and thus a greater penetration distance. In comparison, Figure 4b shows this effect on **TR3**, which is noticeably carried further, presumably due to its smaller molecular size and slightly positive electrophoretic mobility.

Intensity profiles for the 0% acrylate-content hydrogel (ζ = -0.25 mV) would be expected to be similar to that for diffusion alone in the absence of electrophoresis. However, the penetration distance is larger than that for diffusion alone for the solute **TR70**, which has a negligible electrophoretic mobility. It is possible that there is a contribution from pressure-induced flow in this case. For **TR3,** there is a significant contribution to the mass transport from electrophoresis, as well as a potential contribution from pressure-induced flow.

Effect of current on concentration and Pe

Figure 5 shows the intensity at $\rho = 1$ (I_0, eq 14) and Pe_E as functions of current. In these experiments, the tip size, camera exposure time (to assure comparability of intensities), and hydrogel were all held constant. Each data point represents a mean ± **SEM** (see Table S1, entries 2, 3, 5, 7, 8, and 9 for details). An increase in current yields an approximate linear increase in I_0, and thus the concentration of ejected solute. The increase in intensity with an increase in current is not explained based on eq 14. However, eq 14 was derived without taking into account the complex details of the boundary between the fluid inside the pipette and the fluid outside the pipette and in the hydrogel or tissue. The boundary condition is simply that at steady state there exists a constant concentration at $\rho = 1$. The dependence of this value, C_0 or I_0, on conditions is currently under investigation. Figure 5 also shows an approximately linear increase of Pe_E as a function of current. This implies that the solute penetration distance depends linearly on current when Pe_E is greater than about 5 (i.e., e^{-Pe} becomes small). This can be understood by once again considering dimensionless distances corresponding to a particular fraction, *f*, of the background corrected intensity at $\rho = 1$ ($I = I_0 - I_1$). Let us use ρ_f to represent the penetration distance at which $(I-I_1)/I_0$ is *f*. Rearrangement of eq 14 (and analogously, eq 13a) leads to

$$\rho_f = \frac{Pe_E}{\ln(1/1 - f)} \tag{15}$$

We see that the penetration distance, ρ_f, is linearly proportional to Pe_E (and numerically equal to Pe_E when *f* is 0.63), and therefore current. Thus, controlling the current controls the degree of solute penetration. To our knowledge, many have observed this phenomenon in brain tissue iontophoresis, but have not shown the quantitative linear correlation of penetration distance with current.[20,41]

Time to steady state

The time to steady state is roughly correlated with the solute's (**TR70**) penetration distance. In an electrochemical context, Zoski et al. have determined the time to reach a given fraction of the steady state current or potential for spherical and disc microelectrodes under galvanostatic and potentiostatic conditions in which diffusion alone transports solute.[42] For a constant current flowing at a hemispherical microelectrode, analogous to the data reported here, the time depends on the diffusion coefficient of the solute and the size of the electrode. With a tip (i.e., hemispherical electrode) radius of 2 μm and the diffusion coefficient of **TR70**, the time to reach 90% of the steady state condition in the galvanostatic context is about 3 seconds, and to reach 95% is about 14 seconds. These times are short in comparison to our observations of transport from a hemispherical source by both diffusion and electrokinetic processes (several minutes, see SI). This is of course related to the greater distances involved here in contrast to a diffusion-only experiment.

Comparison of Pe_E with Pe_T

In any given experiment, there is one tip radius, one diffusion coefficient, and in principle one solute velocity at $\rho = 1$. Any given experiment therefore has one value of Pe. Consequently, Pe_E (eq 14) and Pe_T (eq 6) should be the same. Figure 6 shows that Pe_E

correlates linearly with Pe_T. The resulting linear regressions for **TR70** and **TR3** had respective slopes of 1.7 and 5.9 and intercepts of 4.2 (borderline significance, $p = 0.055$) and 11.4. Labels refer to rows in Table S1. Among the factors that may be responsible for the lack of unit slope are the varying porosities of the media supporting EOF, uncertainty about the tip size and shape, the assumption (made for mathematical simplicity) that the current emanates from a hemisphere, uncertainly about pressure-induced flow, and the tortuosity of the medium. We will consider each of these.

Porosity is not likely to be a factor. The ratio of Pe_E and Pe_T is the same for an OHSC (porosity ~ 0.2[16]) and hydrogel (porosity > 0.95[32]), indicating the slope is not dependent on porosity. Furthermore, in simple models of porous media, volume-averaged electrokinetic velocity is unaffected by changes in porosity.[43,44] This is because the decrease in porosity increases the electric field in the fluid (because the current density increases due to the decreased cross sectional area of the porous space) and thus the local EOF increases within the porous space, but at the same time the fraction of the porous medium that is fluid, and thus is moving, decreases by exactly the same factor. Thus, the average velocity estimated as the volumetric flow rate divided by the total (porous and nonporous) cross sectional area does not change.

The uncertainty about the position and shape of the tip may be a factor in the slope of the plots in Figure 6. The pipette tip opening, tapering, and ζ-potential influence the electric field in the medium. The current source at the tip is approximated by a hemisphere to simplify the derivation of the steady state concentration profile. In order to obtain intensity-distance profiles from images, we must accurately find the location of $\rho = 1$. We have calculated that an error of ± 1 μm in determining the position of $\rho = 1$ away from a typical 2 μm radius pipette tip opening leads to a 5 to 10% error in Pe_E. As the location of $\rho = 1$ is visual, there may be a systematic error the estimation of that point. Furthermore, as there is in the solution of the analogous diffusion problem, there is likely to be a difference in the numerical constant relating flux from a disc and from a hemisphere. As the tip position is hard to ascertain and shape of the current source at the tip is neither strictly a planar disc nor a hemisphere, there is the possibility of a systematic error as well as random error in the use of the hemispherical geometry in the derivation of eq 14.

A pressure may arise from a ζ-potential mismatch of the pipette and the hydrogel matrix, which is not accounted for in Pe_T[45]. Most hydrogels and the OHSC have different ζ-potentials from the pipette. A pressure gradient arises in the case of mismatched ζ-potentials because the law of conservation of mass requires pressure to compensate for differences in EOF in two adjacent media. For example, for a neutral solute being ejected into a neutral hydrogel, Pe_T is zero. However, the negative ζ-potential in the pipette will create a positive pressure at the tip-hydrogel interface, creating pressure-induced flow into the hydrogel. The magnitude of the pressure depends on many factors other than the ζ-potentials, so estimating the pressure from parameters of the experiment is difficult. Nonetheless, as there is a pressure-induced velocity when Pe_T is zero, the y-intercept in Figure 6 is likely to be a reflection of the pressure at the pipette/ hydrogel interface and thus the ζ-potential mismatch.

Finally, there is the issue of the tortuosity of a medium that impedes solute motion in comparison to free solution. Tortuosity as used here contains effects due to the random changes in a molecule's path dictated by the structure of the medium as well as molecular-scale friction and steric factors.[46] We have assumed that electrokinetic velocity (the sum of v_{ep} and v_{eo}) will be impeded by tortuosity to the same degree as the diffusion coefficient, D. Thus, the value of Pe, and therefore the concentration profile, should not depend at all on tortuosity. The slopes of Figure 6 give us reason to question this assumption. The measured tortuosities[32] are solute and hydrogel dependent (**TR70** 25% hydrogel: 1.97; 0% hydrogel:

2.43; **TR3** 25% hydrogel: 1.02; 0% hydrogel: 1.11). However, the hydrogel porosity is unfortunately correlated with ζ-potential because the more ionic and thus higher ζ-potential hydrogel swells more than the neutral, near zero ζ-potential hydrogel. Thus, experimental testing of this idea is not straightforward. The potentially systematic but unknown errors in determining the electric field strength, in determining the location of ρ = 1, and pressure effects lead to a scaling factor that should not depend on molecular weight of the solute. The difference in the behavior of **TR70** and **TR3** shown in Figure 6 is related to molecular weight, and thus likely due to the tortuosity effects described above. The role of molecular-weight dependent friction in the observed phenomena is under investigation.

Figure 7 shows fluorescence and bright field image overlays of a representative 0.5 μA ejection of **TR70** into the CA1 region of an OHSC at t = 0 and 120 seconds. In this particular experiment, curve fitting reveals that Pe_E is 31, while for the set of all thirty-one ejections Pe_E is 29.4 ± 1.2 (SEM). From a practical perspective, the radius of the ejected **TR70** solution appears to be about 85 μm, demonstrating significant penetration distances. Ejections into the CA1 regions of OHSCs (0.5 μA for 300 seconds) resulted in no significant cell death over controls (experiments: -6 ± 4% cell death; negative control: 0%, positive control: 100%). Thus, under these conditions there is no significant damage to cells caused by the iontophoresis.

Pe_E of **TR70** ejections in OHSCs, fall directly in line with Pe_E determined in hydrogels (Figure 6), indicating the hydrogels are viable models for OHSCs. However, ejections in OHSCs show an increased time to reach steady state than in comparable, 25% acrylate-content hydrogels. This may be an artifact of the tissue dimensions. The OHSC is only about 150 μm thick[47]. Our derivation assumes a spherically symmetrical field and concentration profile. It is the spherical symmetry itself that allows the steady state to be attained. When the distance traveled in the OHSC reaches distances on the order of 100 μm (ρ ~ 50) we can no longer apply the assumption of spherical symmetry, thus we do not expect to see a clear steady state. Hydrogel samples were much thicker (6 mm), so the ejection in them is spherically symmetrical.

Small, highly charged solute

We used tris(2,2'-bipyridine)ruthenium, $Ru(bpy)_3^{2+}$, to determine the effect of matrix ζ-potential on a solute that has a significant electrophoretic mobility and small size. Transport of $Ru(bpy)_3^{2+}$ is affected by the hydrogel ζ-potential similarly to the dextran solutes. When distances are compared at 25% of the maximum intensities, ejections of $Ru(bpy)_3^{2+}$ solution into -22 mV ζ-potential hydrogel (Pe_E = 51) reach 1.5 times further than ejections into -0.25 mV ζ-potential hydrogel (Pe_E = 24). $Ru(bpy)_3^{2+}$ was also used to investigate the effect of ionic strength on the solute ejection. Steady state ejections into the same large ζ-potential hydrogel in a 5 mM HEPES, 5 mM NaCl buffer (Pe_E = 88) travels 1.8 times further than $Ru(bpy)_3^{2+}$ in a 5 mM HEPES, 150 mM NaCl buffer (Pe_E = 51). Solutes can be transported further by decreasing the electrolyte concentration. Many researchers use low ionic strength solutions for iontophoretic delivery of small charged molecules.[27,48] The electrical double layer thickness is proportional to the reciprocal square root of ionic strength. Consequently, the absolute value of the ζ- potential increases with decreasing ionic strength. Hence, the 5 mM NaCl $Ru(bpy)_3^{2+}$ solution creates a more negative ζ-potential than the 150 mM NaCl solution. As a result, the solute penetration distance is greater in the former than the latter.

Impact on quantitative iontophoresis

Herr and Wightman[19,27] have recently developed a method to correct for the effects of the *capillary* EOF on the iontophoresis of neuroactive compounds. Calibrants are iontophoresed into artificial cerebral spinal fluid *in vitro* and detected quantitatively at a microelectrode.

The result is a linear calibration of the rate of iontophoretic injection of solutes relative to a neutral standard vs. the electrophoretic mobility of the solutes. The rate of iontophoretic injection of any compound with a known electrophoretic mobility can then be ascertained experimentally based on the rate of iontophoretic injection of the neutral standard and the established correlation of rate vs. mobility. The approach is a major step forward in making iontophoresis quantitative. However, as we show here, the ζ-potential of the medium has a significant, even dominant, role in the solute distribution in hydrogels and by inference in tissue. Thus, we recommend that the iontophoresis calibration be performed *in vivo* or in a hydrogel model of tissue.

Conclusion

The major conclusion is that under appropriate conditions, the transport of a solute from a small source into a much larger porous, aqueous medium depends strongly on the ζ-potential of the medium. We demonstrated that solute ejection distance is affected by the solute, the solute-containing medium's ionic strength, and hydrogel properties, as well as the current. Pe_E, obtained from experimental intensity- distance plots, is linearly correlated to Pe_T obtained from measureable parameters. OHSCs experience no more cell death than controls following long-term electrokinetic ejection. Thus, this technique is applicable to living tissue for long-distance solute transport.

Supplementary Material

Refer to Web version on PubMed Central for supplementary material.

Acknowledgments

We would like to thank the National Center for Research Resources (UL1 RR024153) and the National Institute of General Medical Sciences (R01 GM044842) for financial support. We are grateful to Prof. Henry White for discussions of the derivation of a concentration profile from mass transport eqs.

LITERATURE CITED

1. Dehghan MHG, Mouzam MI. International Journal of Health Research. 2008; 1:115.
2. Srinivasan V, Higuchi WI. Int. J. Pharm. 1990; 60:133.
3. Pikal MJ. Adv. Drug Del. Rev. 2001; 46:281.
4. Uitto OD, White HS. Pharm. Res. 2003; 20:646. [PubMed: 12739774]
5. Abla N, Naik A, Guy RH, Kalia YN. J. Controlled Release. 2005; 108:319.
6. Santi P, Guy RH. J. Controlled Release. 1996; 38:159.
7. Hao J, Li SK, Liu C-Y, Kao WWY. Exp. Eye Res. 2009; 89:934. [PubMed: 19682448]
8. Stone, TW. Microiontophoresis and pressure ejection. Vol. 8. Chichester; Wiley: 1985.
9. LeBeau FEN, Malmierca MS, Rees A. J. Neurosci. 2001; 21:7303. [PubMed: 11549740]
10. Bloom FE. Life Sci. 1974; 14:1819. [PubMed: 4368008]
11. Shoemaker WJ, Balentine LT, Siggins GR, Hoffer BJ, Henriksen SJ, Bloom FE. J. Cyclic Nucleotide Res. 1975; 1:97. [PubMed: 4474]
12. Purves R. Trends Neurosci. 1980; 3:245.
13. Chen KC, Nicholson C. J. Neurosci. Methods. 2002; 122:97. [PubMed: 12535769]
14. Hrabetova S, Masri D, Tao L, Xiao F, Nicholson C. J. Physiol. (Lond). 2009; 587:4029. [PubMed: 19546165]
15. Dionne VE. Biophys. J. 1976; 16:705. [PubMed: 938714]
16. Sykova E, Nicholson C. Physiol. Rev. 2008; 88:1277. [PubMed: 18923183]
17. Armstrong-James M, Fox K, Kruk ZL, Millar J. J. Neurosci. Methods. 1981; 4:385. [PubMed: 7321578]

18. Armstrong-James M, Millar J, Kruk ZL. Nature. 1980; 288:181. [PubMed: 7432519]
19. Herr NR, Daniel KB, Belle AM, Carelli RM, Wightman RM. ACS Chemical Neuroscience. 2010; 1:627. [PubMed: 21060714]
20. Purves RD. J. Neurosci. Methods. 1979; 1:165. [PubMed: 544961]
21. Trubatch J, Van Harreveld A. J. Theor. Biol. 1972; 36:355. [PubMed: 5073923]
22. Norman RS. J. Theor. Biol. 1975; 52:159. [PubMed: 1152479]
23. Lux HD, Neher E. Exp. Brain Res. 1973; 17:190. [PubMed: 4714525]
24. Nicholson C, Phillips JM, Gardner-Medwin AR. Brain Res. 1979; 169:580. [PubMed: 445169]
25. Curtis DR, Perrin DD, Watkins JC. J. Neurochem. 1960; 6:1. [PubMed: 13718945]
26. Fregni F, Boggio Paulo S, Nitsche Michael A, Rigonatti Sergio P, Pascual-Leone A. Depress. Anxiety. 2006; 23:482. [PubMed: 16845648]
27. Herr NR, Kile BM, Carelli RM, Wightman RM. Anal. Chem. 2008; 80:8635. [PubMed: 18947198]
28. Guy Y, Muha RJ, Sandberg M, Weber SG. Anal. Chem. 2009; 81:3001. [PubMed: 19298057]
29. Guy Y, Sandberg M, Weber SG. Biophys. J. 2008; 94:4561. [PubMed: 18263658]
30. Xu H, Guy Y, Hamsher A, Shi G, Sandberg M, Weber SG. Anal. Chem. 2010; 82:6377. [PubMed: 20669992]
31. Drouin H. Biophys. J. 1984; 46:597. [PubMed: 6498272]
32. Faraji AH, Cui JJ, Guy Y, Li L, Gavigan CA, Strein TG, Weber SG. Langmuir. 2011; 27:13635. [PubMed: 21905710]
33. Noraberg J, Kristensen BW, Zimmer J. Brain research protocols. 1999; 3:278. [PubMed: 9974143]
34. Stoppini L, Buchs PA, Muller D. J. Neurosci. Methods. 1991; 37:173. [PubMed: 1715499]
35. Hamsher A, Xu H, Guy Y, Sandberg M, Weber SG. Anal. Chem. 2010; 82:6370. [PubMed: 20698578]
36. Barz DPJ, Vogel MJ, Steen PH. Langmuir. 2009; 25:1842. [PubMed: 19170651]
37. McGuffin VL, Tavares MFM. Anal. Chem. 1997; 69:152.
38. Thormann W, Zhang C-X, Caslavska J, Gebauer P, Mosher RA. Anal. Chem. 1998; 70:549. [PubMed: 21644753]
39. Scales N, Tait RN. J. Chem. Phys. 2006; 125:094714/1. [PubMed: 16965112]
40. Probstein, RF. Physicochemical Hydrodynamics, An Introduction: Second Edition. 1994.
41. Krnjević K. The Journal of Physiology. 2010; 588:33. [PubMed: 19822549]
42. Zoski CG, Bond AM, Allinson ET, Oldham KB. Anal. Chem. 1990; 62:37.
43. Barrande M, Bouchet R, Denoyel R. Anal. Chem. 2007; 79:9115. [PubMed: 17979254]
44. Scales N, Tait RN. Journal of Chromatography, A. 2008; 1205:150. [PubMed: 18722624]
45. Rathore AS, Horvath C. Anal. Chem. 1998; 70:3069. [PubMed: 9684553]
46. Westerhuis WH, Sturgis JN, Niederman RA. Anal. Biochem. 2000; 284:143. [PubMed: 10933867]
47. Guy Y, Rupert AE, Sandberg M, Weber SG. J. Neurosci. Methods. 2011; 199:78. [PubMed: 21497166]
48. Slais K, Vorisek I, Zoremba N, Homola A, Dmytrenko L, Sykova E. Exp. Neurol. 2008; 209:145. [PubMed: 17961555]

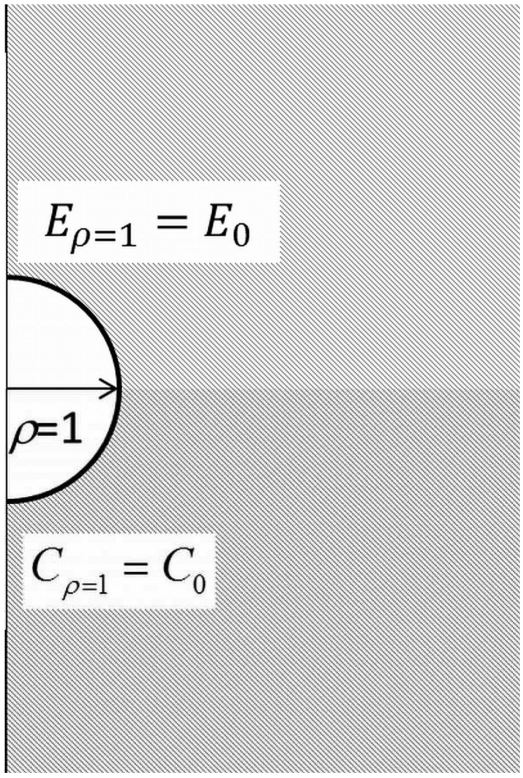

Figure 1.
Geometry used to derive eq 13. The hemispherical source has a dimensionless radius of unity. The flux from the tip goes into the porous medium (gray). At the boundary, the field and concentration are specified.

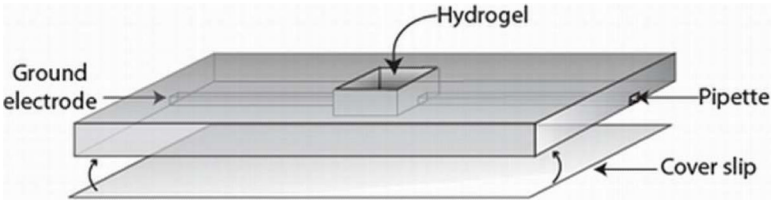

Figure 2.

Hydrogel cell. A coverslip was super-glued to the base of the upper PVC piece. An approximately 6 mm thick hydrogel square was placed in the center space of the cell. A pulled borosilicate pipette filled with fluorophore solution was inserted into the cell and hydrogel through the channel. A ground electrode (Ag) was inserted into the hydrogel from the opposite side.

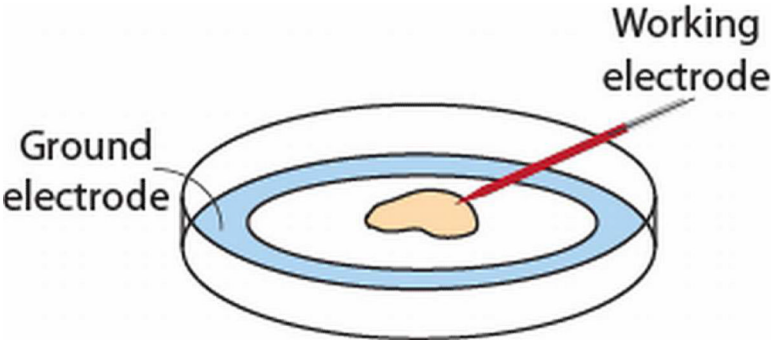

Figure 3.
OHSC experimental setup. An OHSC and its attached membrane are placed over HBSS in a dish. A ground electrode is placed remotely in the bath. A working electrode is placed distally in a borosilicate pipette that is inserted into the OHSC at a 20° angle.

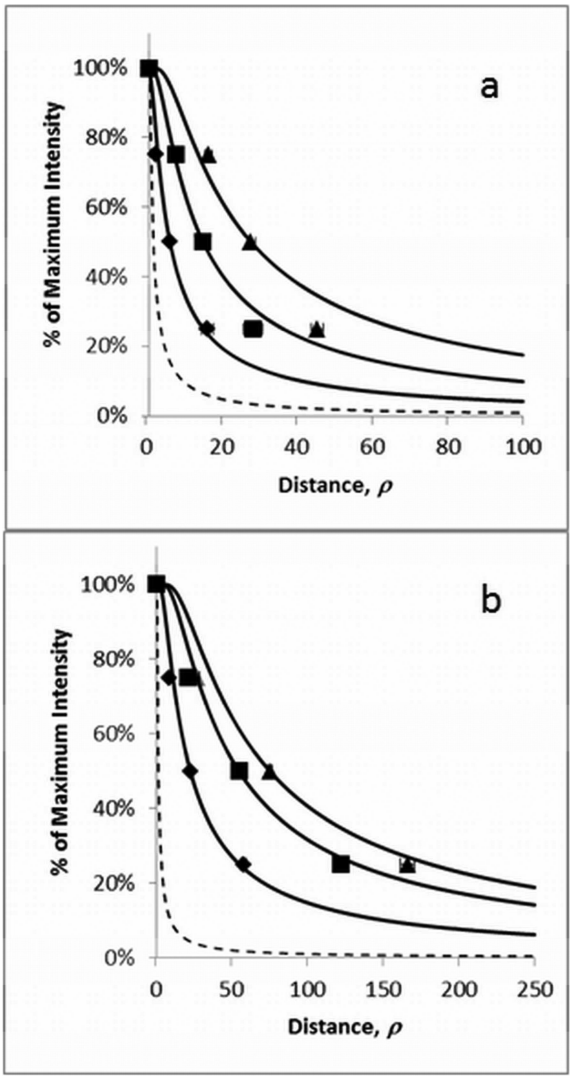

Figure 4.

a) Fluorescence intensity vs. dimensionless distance for **TR70**. Data points represent average values of distance ρ at $I(\rho)/I_0$ = 1, 0.75, 0.50, and 0.25 based on about 10 repeats (see Table S1 for actual values). The smooth curves are based on eq 14 passing through the data points at $I(\rho)/I_0$ = 1 and 0.50. Hydrogel ζ-potentials: -0.25 mV (◆); -9.5 mV (■); -23.0 mV (▲). The dashed line corresponds to the expected profile for diffusion only. B) Fluorescence intensity vs. distance for **TR3**. Same as for 3 a, except the hydrogel ζ-potentials are -0.25 (◆); -15.2 (■); -24.7 (▲) mV. Note the difference in the x-axis scale.

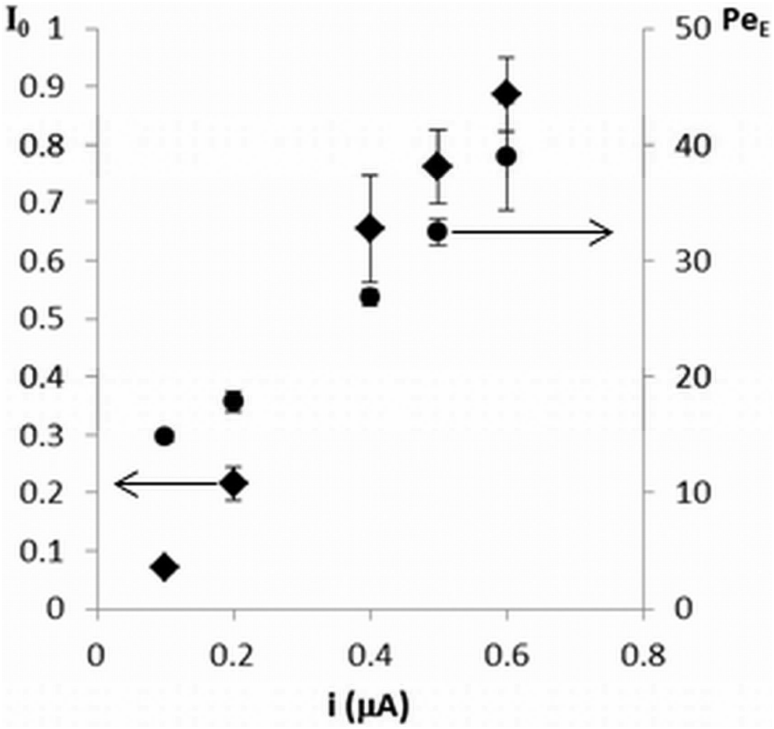

Figure 5.

Effect of current on I_0 and Pe_E horizontal axis represents the current used to eject potential hydrogel. **TR70** into a -24.7 mV ζ- Diamonds correspond to the steady state values of I_0 and the left ordinate. Circles correspond to Pe_E and the right ordinate).

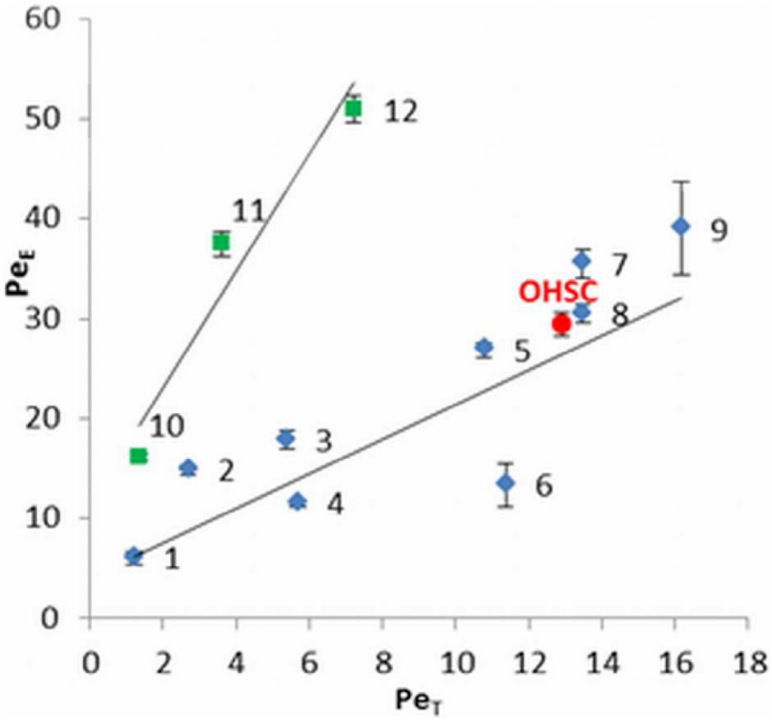

Figure 6.

Steady state Pe_E vs. Pe_T: Blue diamonds (◆) represent **TR70**; green squares (■) represent **TR3**; and the red dot represents **TR70** in the OHSC. More details are provided in Table S1. Numbers beside the points correspond to rows in Table S1 and also indicate conditions as follows: hydrogel (% acrylic acid)/current (μA) **1**:0/1; **2**:25/.1; **3**:25/.2; **4**:10/.5; **5**:25/.4; **6**:10/1; **7**:25/.5; **8**:25/.5; **9**:25/.6; **10**:0/1; **11**:10/.5; **12**:10/1.

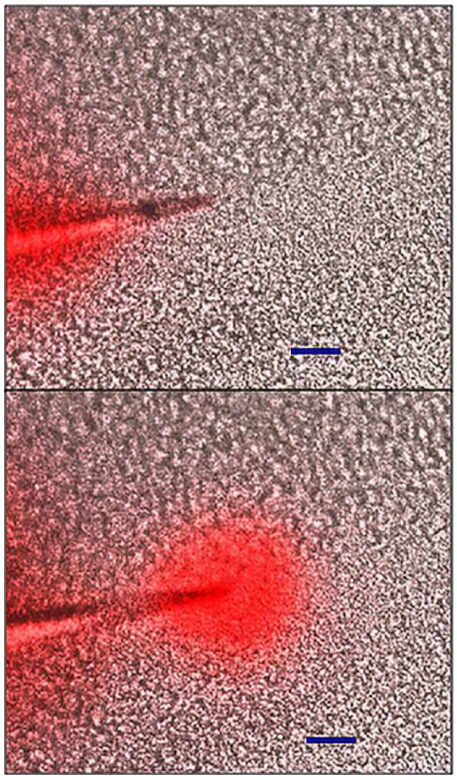

Figure 7.
Injections into an OHSC: Fluorescence images overlaid on bright field images of a 0.5 μA ejection of **TR70** into the CA1 region of an OHSC. Top: t = 0 seconds. Bottom: t = 120 seconds. The scale bar represents 50 μm.

Table 1

Free solution diffusion coefficients and electrophoretic mobilities of the fluorophores used.

Fluorophore	**Abbreviation**	**Free Solution Diffusion Coefficient ($D/10^{-10}$ m^2/s)[a]**	**Electrophoretic Mobilities ($\mu_{ep}/10^{-9}$ m^2/Vs)[a]**
Texas Red dextran conjugate 70 kDa	**TR70**	0.37 ± 0.02[c] (N = 32)[b]	0.46 ± 0.03[c] (N = 3)[b]
Texas Red dextran conjugate 3 kDa	**TR3**	1.05 ± 0.05[c] (N = 48)	2.56 ± 0.04 (N = 3)
Tris(2,2'-bipyridine)ruthenium(III)	$Ru(bpy)_3^{2+}$	3.70 ± 0.34 (N = 48)	25.86 ± 0.02 (N = 3)

[a] Each entry is a mean ± standard error of the mean (SEM).

[b] Number of replicates.

[c] Previously reported in Faraji *et al.*[32].